Dimensional Assessment and Error Analysis of 3D CAD Models Manufactured with Bound Metal Deposition

Yasya Khalif Perdana Saleh[1,3,4], Rifky Ismail[1,2,*], Jamari Jamari[1], I Nyoman Jujur[3,*], Poki Agung Budiantoro[5], Sri Ramayanti[5], Rochmad Winarso[6]

[1]Department of Mechanical Engineering; [2]Center for Biomechanics, Biomaterial, Biomechatronics, and Biosignal Processing (CBIOM3S), Diponegoro University, Semarang, Indonesia

[3]Biocompatible Material, National Research and Innovation Agency, Tangerang Selatan, Indonesia

[4]Department of Mechanical Engineering, Universitas Global Jakarta, Jakarta, Indonesia

[5]Satellite Technology Center, National Research and Innovation Agency, Bogor, Indonesia

[6]Department of Mechanical Engineering, Faculty of Engineering, Muria Kudus University, Kudus, Indonesia

Received 23 July 2025; received in revised form 24 October 2025; accepted 30 October 2025

DOI: https://doi.org/10.46604/ijeti.2025.15439

Abstract

This study evaluates dimensional deviations of 316L stainless steel components produced using the Bound Metal Deposition (BMD) method. The evaluation covers four production stages: CAD modeling, slicing, printing, and sintering. The approach involves experimental measurements and finite element simulations to assess accuracy. Results indicate an average dimensional deviation of 6%, with height-related features showing the most significant errors due to anisotropic shrinkage and inconsistencies in layer deposition. The widely used 1.16 scale factor is inadequate for precise dimensional recovery. Instead, a revised scale factor of 1.13 is developed through empirical analysis and validated using ANSYS simulation. This new factor shows better agreement with the original CAD design. Furthermore, the achieved dimensional accuracy falls within clinically accepted tolerances for dental implants (0.19-0.36 mm), making it suitable for biomedical applications. Overall, these findings provide a validated framework for dimensional calibration in BMD, improving the accuracy of patient-specific medical devices.

Keywords: Bound Metal Deposition, dimensional accuracy, 3D printing, stainless steel 316L

1. Introduction

An implant is a medical device designed to replace or support the function of a specific body part, such as in orthopedics, dentistry, and reconstructive surgery [1]. One of the implant materials still in use today is SS316L stainless steel due to its biocompatibility, high mechanical strength, and corrosion resistance [2]. On the other hand, the current demand for implants is focused on adequate material properties, ease of manufacturing, and size accuracy, which are crucial factors for future implant development. Advances in technology, particularly in metal 3D printing, have enabled the production of customized implants. This technology allows for printing complex designs more easily and efficiently than conventional methods. Several types of metal 3D printing technologies, such as Selective Laser Melting (SLM), Direct Metal Laser Sintering (DMLS), Binder Jetting (BJ), Powder Bed Fusion (PBF), Directed Energy Deposition (DED), Fused Filament Fabrication (FFF), Fused Deposition Modeling (FDM), and Material Jetting, have been applied for implant fabrication [3].

* Corresponding author. E-mail address: rifky_ismail@ft.undip.ac.id; inyo002@brin.go.id

One emerging 3D metal printing technology is the Bound Metal Deposition (BMD) method [4]. This method is an extrusion-based 3D printing process for metals, where components are created by depositing metal powder bound together with a polymer binder [5]. With this method, production costs can be reduced by 60-80% compared to the Selective Laser Sintering (SLS) and Electron Beam Melting (EBM) processes [6]. This presents an opportunity for the BMD method to become an alternative for printing implants with complex shapes. The BMD printing process consists of three main stages. The first stage is the printing process, where the material is bonded in powder form using a polymer binder. The second stage is debinding, in which the polymer binder is removed at a specific temperature. The final stage is sintering, where the material is heated at a controlled temperature, allowing metal particles to fuse into a solid structure. Before printing, parameter settings for the BMD process must be configured.

One of these parameters includes an automatic scale factor applied during printing to compensate for shrinkage during sintering, ensuring the final product matches the CAD model dimensions. However, the exact scale factor for printing and shrinkage during sintering is not always predictable, as there are no precise control mechanisms to guarantee that the printed part expands correctly or shrinks to match the intended CAD dimensions. This uncertainty highlights the need for a dimensional assessment to evaluate errors in the final product after printing. The urgency of such research lies in minimizing deviations and optimizing CAD model designs to accommodate the characteristics of BMD 3D metal printing. Ensuring dimensional accuracy is crucial, particularly for implant manufacturing, where precise shape and size are essential for successful application.

Research using the BMD method remains limited, particularly in dimensional assessment. Previous studies on BMD have primarily focused on mechanical testing, material characterization, and environmental effects. Researchers such as Iacopo et al. [5] and Watson et al. [6] evaluated the ecological impact and mechanical properties of 17-4 PH stainless steel components produced through BMD 3D printing. Their study compared two scenarios: sintered and heat-treated samples using the Life Cycle Assessment (LCA) methodology to analyze sustainability, energy consumption, and tensile properties [5-6]. Bjørheim and Lopez [7] investigated the mechanical properties and fatigue capacity of 17-4 PH stainless steel specimens produced using the BMD method, revealing that the material exhibits anisotropic behavior and defect networks, such as cracks, influenced by printing orientation, with XY-flat specimens showing the highest tensile strength.

Meanwhile, Campbell et al. [8] focused on the design and fabrication of a functional Beta Stirling Engine (BSE) using the BMD process with 17-4 PH stainless steel, addressing challenges related to geometric accuracy, heat transfer, and thermal expansion. Luchinsky et al. [9] focused on a multi-scale physics-based approach to modeling nonlinear shrinkage during BMD manufacturing, addressing phenomena ranging from atomistic dynamics to full-part shrinkage and estimating key parameters such as grain boundary width, surface diffusion coefficient, and sintering stress.

Although several studies have investigated and optimized the fabrication of SS316L components using other AM techniques, such as DMLS for dimensional accuracy testing [10] and BJ for parameter optimization [11] and sintering densification through dimensional compensation [12], these works focus primarily on PBF- and binder-based processes. None has specifically addressed dimensional accuracy in the BMD method, which involves extrusion and sintering mechanisms distinct from DMLS and BJ. Unlike those studies, the present work conducts a full-chain dimensional assessment across design, slicing, printing, and sintering stages, and introduces an experimentally validated scale factor to directly address shrinkage behavior in BMD.

Dimensional deviations in 3D-printed implants critically influence clinical fit and long-term functionality, particularly in orthopedic and dental applications. In orthopedics, poor dimensional accuracy can impair mechanical stability and lead to complications such as wound dehiscence, infection, and implant dislocation [13]. In dental implants, even sub-millimeter deviations can disrupt implant placement accuracy, affect occlusion, and compromise oral health outcomes [14-15]. While maximum allowable errors are not universally defined for orthopedic implants, minimizing dimensional inaccuracies remains essential [13]. In dental contexts, deviations of 0.19-0.23 mm for entry point offsets and 0.32-0.36 mm for apex offsets are considered clinically acceptable [14], and general deviations of up to 0.26 mm are still within tolerance for dental models [16]. These constraints highlight the urgency for manufacturing methods like BMD that can achieve precise, consistent output for biomedical applications.

In comparison with other additive manufacturing techniques, SLM generally provides higher dimensional accuracy due to precise process control, but it involves higher costs and energy consumption. BJ offers lower production costs and faster build rates, yet it often exhibits anisotropic shrinkage during sintering that complicates dimensional recovery. Meanwhile, Metal Injection Molding (MIM) achieves consistent accuracy for mass production but lacks flexibility for patient-specific customization. BMD, therefore, occupies an intermediate position that is cost-effective but requires robust scale factor calibration to achieve clinically acceptable tolerances [17].

No prior study has provided a full-chain dimensional analysis from CAD design through slicing, printing, and sintering in the BMD process, nor proposed a refined, experimentally validated scale factor with clinical relevance. Furthermore, current research lacks a geometry-aware evaluation of error propagation that considers physical measurements and simulation-based verification. While prior studies have investigated shrinkage modeling and compensation strategies in BMD [9] and BJ [12, 18], these works focused on specific aspects of the process (e.g., sintering shrinkage or feature-level deviations) rather than the entire fabrication chain. The novelty of the present study lies in providing a comprehensive, stage-by-stage dimensional analysis covering the design, slicing, printing, and sintering stages, validated by both experimental measurements and finite element simulation, and explicitly benchmarked against clinically accepted tolerances for biomedical implants.

This study aims to fill this gap by systematically evaluating dimensional deviations across four BMD process stages using SS316L specimens, assessing the implications of dimensional error for implant fit based on known clinical tolerances, and proposing a revised scale factor of 1.13 derived from combined empirical measurements and finite element simulations. These contributions offer a dimensional calibration framework tailored for high-precision applications in the biomedical sector.

2. Materials and Methods

The research process began with the design and fabrication of standardized test specimens intended for evaluating the dimensional behavior of stainless steel 316L using the BMD technique. The workflow covered every stage of the process from digital modeling and slicing to printing, debinding, and sintering, allowing for a comprehensive assessment of dimensional variations. The following subsections describe the materials used and the detailed methods applied during fabrication and measurement.

2.1. Materials

The product design process in this study began with Autodesk Inventor software. The designed products were based on the standard tensile test dimensions according to ASTM E8 and the standard bending test dimensions according to ASTM E290, as shown in Fig. 1.

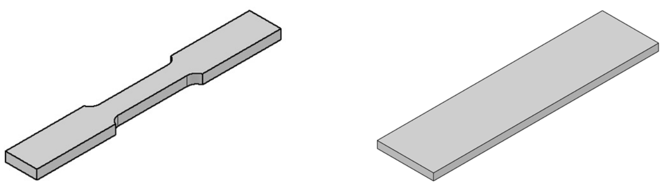

(a) Tensile test (b) Bending test

Fig. 1 Product design

The designed product underwent parameter setting using the Desktop Metal Slicer software, which is directly integrated with the BMD 3D printing system from Desktop Metal. This software serves as the main interface for converting the CAD model into machine-readable instructions, defining parameters such as layer height, nozzle temperature, and infill density. The slicing process also includes automatic scaling to compensate for shrinkage during sintering, as well as the generation of toolpaths for each layer. All process parameters were carefully selected to ensure dimensional accuracy, surface quality, and structural integrity of the printed specimens. The details of the parameters input into the slicer software are summarized in Table 1.

Table 1 Printing parameters

Property	Explanation
Material	Stainless steel 316L
Temperature nozzle	195 °C
Temperature bed/platform	65 °C
Nozzle diameter	250 µm
Layer height	100 µm
Wall Thickness	900 µm
Infill patters	Grid/Lines
Infill density	35%
Print speed	15 mm/s
Sintering scale factor (x,y,z)	1.16

The BMD printing process consists of three main stages: printing, debinding, and sintering, as illustrated in Fig. 2. Each stage represents a critical transformation step, beginning with material deposition, followed by binder removal, and concluding with densification through high-temperature treatment. Together, these stages convert the initial printed structure into a fully dense and mechanically robust metallic component.

Fig. 2 BMD printing stages

During the printing stage, the design was transformed into a physical product. In this process, the printed object was scaled by 1.16, based on the default parameters in the Desktop Metal Slicer software. The debinding process used Trans-dichloroethylene to dissolve the polymer wax coating on the printed part. The final sintering stage strengthened the material by heating it to a specific temperature in an H_2+Ar inert gas environment, allowing the molecules to fuse and enhance its strength [5]. Printing was performed in a temperature-controlled laboratory environment, with the ambient temperature maintained at approximately 25 °C. During printing, the nozzle operated at 165 °C inside a closed build chamber with vacuum/inert gas protection, thereby minimizing the influence of external ambient air.

Exposure to laboratory air occurred only after printing was completed, and specimens were removed only after cooling to room temperature inside the machine to prevent bending or thermal distortion. The sintering process was conducted in the Desktop Metal furnace under an H_2+Ar atmosphere. Although the detailed heating profile is fully automated and not user-configurable, previous studies on BJ and BMD for 316L stainless steel report that sintering is typically performed in the range of 1350-1380 ℃ with controlled heating, holding, and cooling cycles to achieve near-theoretical densification [11-12, 19]. The specifications of the Desktop Metal BMD machine are shown in Table 2.

Table 2 Desktop Metal specifications

Performance	Max build rate	16 cm^3/hr
	Max build weight	6.5 kg in green state
Physical	Build chamber	Heated up to 50 ℃
	Build envelope	28.9 × 18.9 × 19.5 cm
	Build plate	Heated, up to 70 ℃ Vacuum-enabled print bed
	Nozzle diameter (build media)	0.40 mm standard resolution 0.25 mm high resolution
	Power requirements	100-120 VAC, 50/60 Hz, 15 A, 1-phase
Media	Build media	Bound metal rods (metal powder + wax and polymer binder)
	Interface media	Bound metal ceramic rods
	Network connectivity	Wireless and Ethernet
	Software	Fabricate software

2.2. *Methods*

The next step involved the measurement process of the printed and sintered parts, where shape changes occurred during these stages. Fig. 3 illustrates the elements that were measured and compared with the design, manual, and software-based measurements.

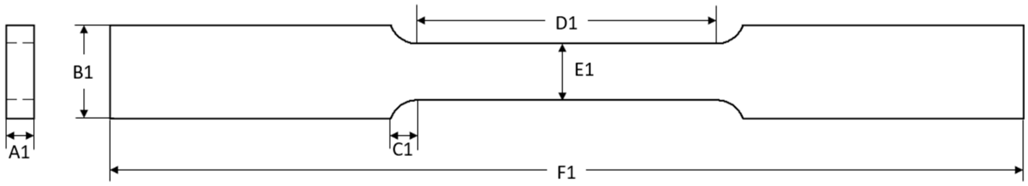

(a) Tensile test specimen

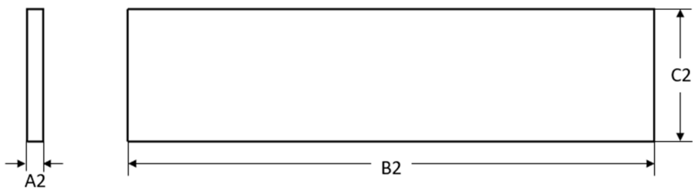

(b) Bending test specimen

Fig. 3 Elements to be measured

Elements A1, B1, C1, D1, E1, and F1, as well as A2, B2, and C2, will be measured across four stages: design, slicing, printing, and sintering. These stages produce varying dimensions due to several influencing factors, which will be analyzed in the measurement results. Therefore, an evaluation is necessary at each stage. Measurements will be conducted using a vernier caliper, with repeated trials to ensure dimensional accuracy. Fig. 4 illustrates the tool used for measuring the specimen.

Fig. 4 Object measurement tool

The final stage involves data analysis, where the dimensions from the software are compared with those of the printed and sintered specimens. The comparison between the slicing and printing results is conducted due to the scale factor applied during printing. In contrast, comparing the original design and the sintered specimen is necessary because the sintering process causes shrinkage to match the initial design dimensions. Each element was measured three times per specimen using the vernier caliper, and the results are presented as mean (±) standard deviation to account for variability and measurement reliability. Fig. 5 illustrates the specimen size changes, explaining why the comparisons are conducted separately.

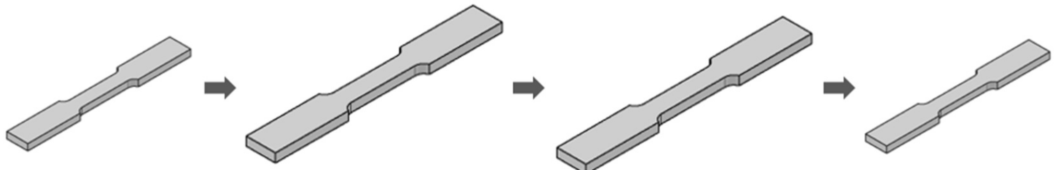

Fig. 5 Specimen size change scheme

3. Results

The experimental findings are organized to demonstrate dimensional variations observed across each stage of the BMD process. Comparative measurements were conducted to evaluate deviations between the CAD design, printed, and sintered specimens, identifying potential sources of dimensional error. The results also emphasize the influence of process parameters, material shrinkage, and geometric complexity on the final accuracy of the printed components, forming the basis for scale factor refinement and dimensional calibration.

3.1. Measurement in the CAD design

Measurement values were obtained in the design process, as shown in Fig. 6, and these values are summarized in Table 3. The CAD model serves as the geometric reference for all subsequent measurements, ensuring that every dimension in later stages can be compared directly with the original design. The measurements correspond to the standardized dimensions defined by ASTM E8 for tensile tests and ASTM E290 for bending tests, ensuring that the designed specimens meet recognized testing criteria. These base values are crucial for identifying deviations introduced during slicing, printing, and sintering. Any difference observed in later stages can therefore be attributed to process-induced variations rather than design inaccuracies. By establishing this baseline, the CAD design provides a control model for validating the dimensional accuracy and scale factor calibration throughout the BMD fabrication workflow.

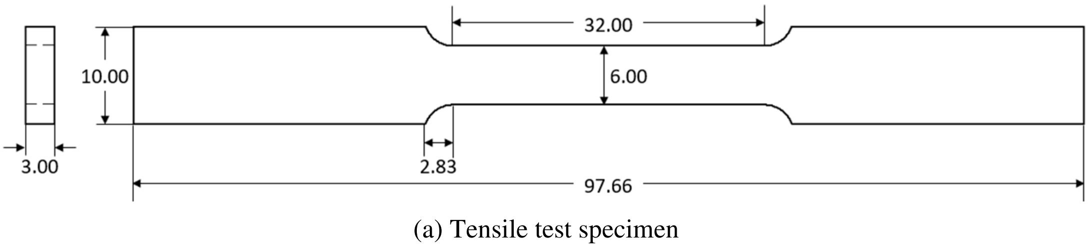

(a) Tensile test specimen

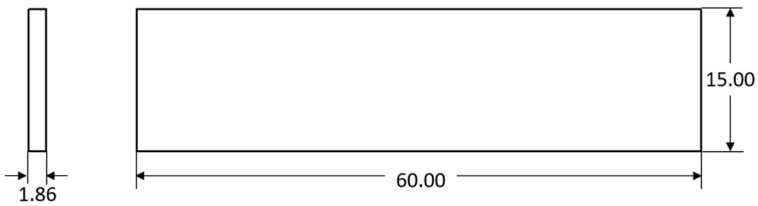

(b) Bending test specimen

Fig. 6 Measurement in the CAD design

Table 3 Desktop Metal specifications

Element	Value
A1	3 mm
B1	10 mm
C1	2.83 mm
D1	32 mm
E1	6 mm
F1	97.66 mm
A2	1.86 mm
B2	60 mm
C2	15 mm

3.2. *Measurement in the slicing process*

In this process, the dimensions are enlarged to account for the shrinkage during sintering, with all dimensions multiplied by a scale factor of 1.16. This automatic adjustment is carried out by the slicing software to anticipate dimensional reduction that occurs during the later sintering phase. By pre-compensating through digital scaling, the process helps maintain the intended geometric fidelity between the CAD model and the final printed part. The scale factor is calculated according to the method described.

$$sf = \frac{D_1}{D_0} \tag{1}$$

where sf is the scale factor, D_0 is the initial dimension, and D_1 is the final dimension.

Table 4 presents the enlarged dimensions in the slicing process. The slicing stage represents a digital compensation phase that anticipates shrinkage occurring during sintering. The automatic scaling applied by the Desktop Metal Slicer ensures that the printed part, after shrinkage, approximates the original CAD geometry. However, the default factor of 1.16 may not precisely correspond to the actual shrinkage behavior of stainless steel 316L, which can vary depending on part geometry, thermal gradient, and binder removal dynamics. Therefore, the data presented in Table 4 form the initial reference for evaluating whether the default scaling parameter adequately compensates for shrinkage, or if further adjustment (such as the proposed 1.13 factor) is required to achieve dimensional conformity in the final sintered product.

Table 4 Desktop Metal specifications

Element	Value
A1	3.48 mm
B1	11.6 mm
C1	3.28 mm
D1	37.12 mm
E1	6.96 mm
F1	113.29 mm
A2	2.16 mm
B2	69.6 mm
C2	17.4 mm

3.3. *Measurement in the printing process*

This process takes place after printing. The BMD method’s printing process applies material extrusion layer by layer to form a specific shape. During printing, the specimen is produced according to the enlarged dimensions from the slicing process, with a scale factor of 1.16 from the original design size. In this stage, three tensile and three bending test specimens are printed, as shown in Fig. 7 and Fig. 8.

(a) Specimen 1 (b) Specimen 2 (c) Specimen 3

Fig. 7 Printed tensile test specimen

(a) Specimen 1 (b) Specimen 2 (c) Specimen 3

Fig. 8 Printed bending test specimen

In the measurement process, two methods are used to compare dimensions: manual measurement and software-based measurement. Each specimen is measured three times to ensure accuracy. Table 5 presents the element dimensions of the printed specimens measured using a vernier caliper.

Table 5 Element dimensions of printed specimen measured with vernier caliper

Elements	Specimen 1 (mm)				Specimen 2 (mm)				Specimen 3 (mm)				Overall average (mm)
	M1	M2	M3	A	M1	M2	M3	A	M1	M2	M3	A	
A1	3.76	3.79	3.70	3.75	3.74	3.77	3.84	3.78	3.70	3.77	3.71	3.73	3.75
B1	11.77	11.79	11.73	11.76	11.87	11.82	11.87	11.85	11.70	11.75	11.77	11.74	11.78
C1	3.18	3.21	3.11	3.17	3.61	3.46	3.37	3.48	3.37	3.38	3.29	3.35	3.33
D1	36.49	36.56	36.40	36.48	36.39	36.43	36.45	36.42	36.44	36.17	36.28	36.30	36.40
E1	7.18	7.18	7.18	7.18	7.30	7.31	7.27	7.29	7.15	7.16	7.17	7.16	7.21
F1	113.02	113.02	113.01	113.02	113.13	113.05	113.10	113.09	113.05	113.03	113.02	113.03	113.05
A2	2.35	2.41	2.41	2.39	2.29	2.36	2.27	2.31	2.21	2.23	2.25	2.23	2.31
B2	69.54	69.56	69.53	69.54	69.73	69.73	69.70	69.72	69.47	69.46	69.48	69.47	69.58
C2	17.53	17.54	17.58	17.55	17.56	17.57	17.55	17.56	17.49	17.50	17.53	17.51	17.54

Table 5 presents Measurement (M) and Average (A), indicating that each specimen and its parts were measured thrice. The measurement results clearly show the differences between them. These variations reflect the influence of printing parameters, dimensional scaling, and potential layer inconsistencies during fabrication. The collected data serve as a quantitative basis for assessing the dimensional accuracy of the BMD process and for identifying elements that exhibit the greatest deviation across specimens.

3.4. Measurement in the sintering process

The sintering stage is the final step in the BMD method, where the material is strengthened by heating it to a specific temperature until its particles fuse. The tensile and bending test specimens undergo shrinkage during this stage, aligning with the original CAD design dimensions. Fig. 9 and Fig. 10 show the tensile and bending test specimens after the sintering process.

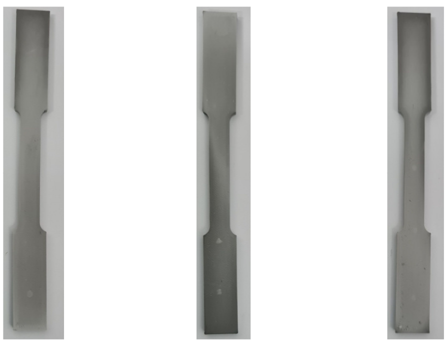

(a) Specimen 1 (b) Specimen 2 (c) Specimen 3

Fig. 9 Sintered tensile test specimen

(a) Specimen 1 (b) Specimen 2 (c) Specimen 3

Fig. 10 Sintered bending test specimen

The measurement process for the sintered specimens follows the same approach as the printed specimens, using manual and software-based measurements. Each specimen is measured three times to ensure accuracy. Table 6 presents the element dimensions of the sintered specimens measured using a vernier caliper.

Table 6 Element dimensions of sintered specimen measured with vernier caliper

Elements	Specimen 1 (mm)				Specimen 2 (mm)				Specimen 3 (mm)				Overall average (mm)
	M1	M2	M3	A	M1	M2	M3	A	M1	M2	M3	A	
A1	3.08	2.97	3.01	3.02	3.00	2.94	3.04	2.99	3.08	2.97	2.99	3.01	3.01
B1	10.33	10.31	10.22	10.29	10.25	10.21	10.23	10.23	10.18	10.22	10.15	10.18	10.23
C1	1.92	1.83	1.87	1.87	1.92	1.88	1.86	1.89	1.82	1.93	1.80	1.85	1.87
D1	32.05	32.17	32.11	32.11	33.10	33.02	33.07	33.06	33.05	33.12	33.03	33.07	32.75
E1	6.22	6.23	6.21	6.22	6.25	6.23	6.24	6.24	6.24	6.18	6.22	6.21	6.22
F1	98.65	98.78	98.70	98.71	98.49	98.69	98.62	98.60	98.63	98.59	98.43	98.55	98.62
A2	1.93	1.82	1.93	1.89	2.17	2.17	2.10	2.15	2.03	1.98	2.02	2.01	2.02
B2	60.47	60.40	60.30	60.39	60.78	60.81	60.82	60.80	60.47	60.56	60.59	60.54	60.58
C2	15.10	14.98	14.99	15.02	15.30	15.33	15.39	15.34	15.25	15.15	15.16	15.19	15.18

All dimensional data in Tables 5 and 6 are reported as mean ± standard deviation (n = 3 specimens × 3 repetitions per element), which provides a measure of variability across the limited sample set. The results indicate that dimensional variations persist even after sintering, primarily due to thermal shrinkage and geometry-dependent densification behavior. These findings serve as a reference for evaluating the effectiveness of the applied scale factor and identifying features most sensitive to shrinkage during the BMD sintering process.

4. Discussion

The discussion section analyzes the dimensional deviations observed across all stages of the BMD process. It aims to interpret the quantitative results obtained from the experimental measurements and to link them with the physical phenomena occurring during printing and sintering. Particular attention is given to identifying factors contributing to shrinkage, anisotropy, and geometric distortion. The findings are compared with existing studies on additive manufacturing to highlight the distinct characteristics of BMD in terms of dimensional stability. Furthermore, this section evaluates the performance of the proposed scale factor and its alignment with clinically acceptable tolerances. The insights derived here provide a scientific basis for improving process calibration and ensuring reliability in medical-grade component fabrication.

4.1. Experiment analysis

The measurement results obtained using a vernier caliper for the printing and sintering processes are compared with the slicing and design stages. Fig. 11 compares the printing measurement results for each element in each specimen using a vernier caliper.

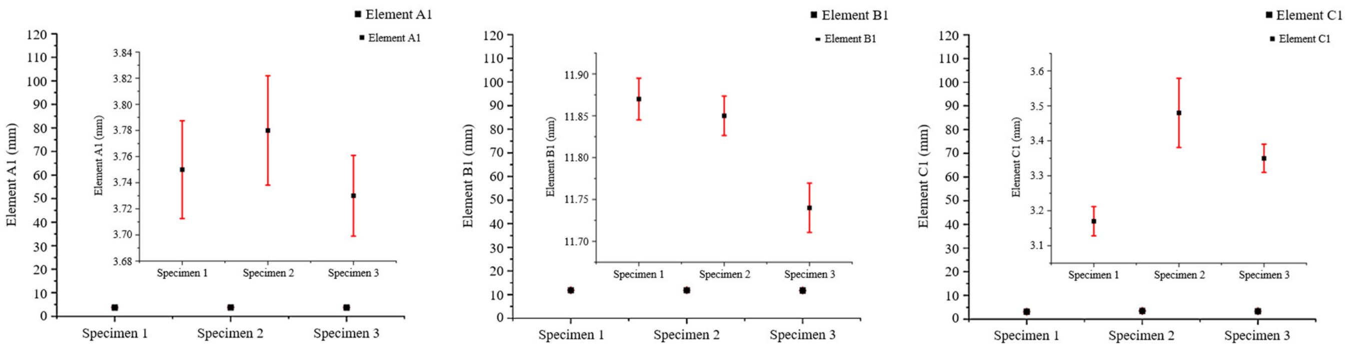

(a) Element A1 (b) Element B1 (c) Element C1

Fig. 11 Comparison of measured dimensions for three printed specimens of each element

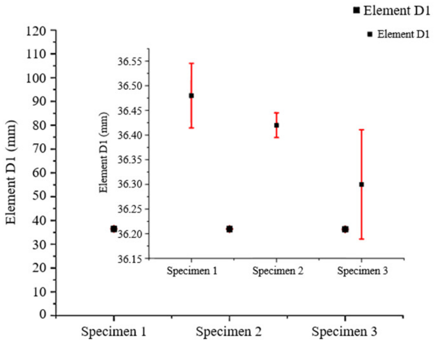

(d) Element D1

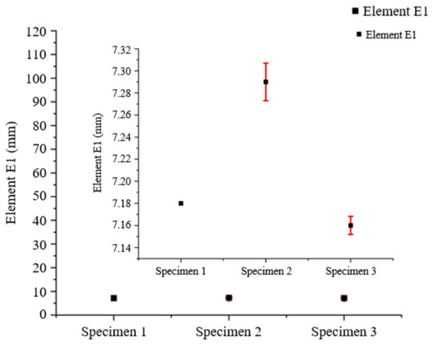

(e) Element E1

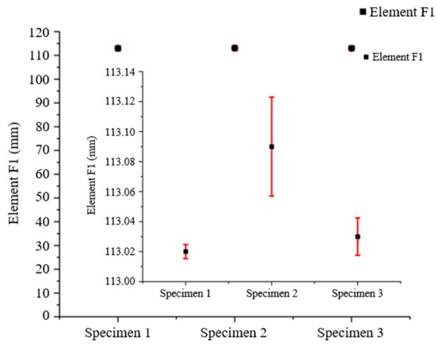

(f) Element F1

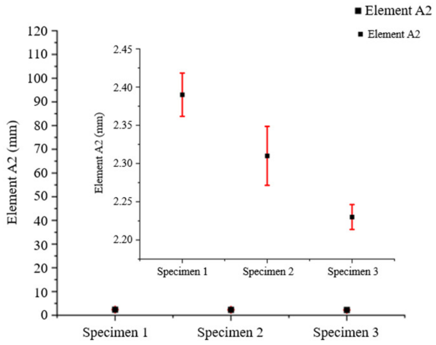

(g) Element A2

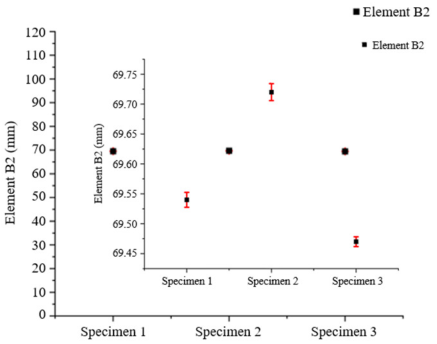

(h) Element B2

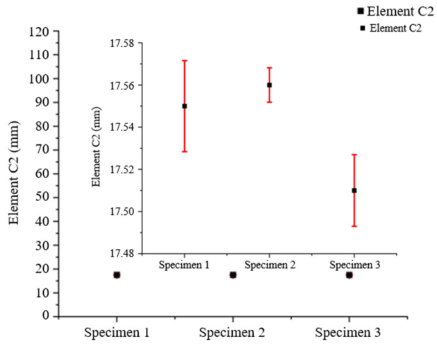

(i) Element C2

Fig. 11 Comparison of measured dimensions for three printed specimens of each element (continued)

Based on the graph in Fig. 11, the size values for each specimen vary, with the most extensive deviation range observed in elements D1 and C1. This is due to the complex positioning required for measurement with a vernier caliper. Various factors, such as the printing position, print speed, nozzle temperature, or environmental conditions during printing, may cause the size differences for each element and specimen. However, despite the deviations, the pattern of variation remains relatively consistent across the specimens. When compared to the measurements from the scale enlargement in the slicing process, there is a difference, but it is not significant. Fig. 12 shows the comparison between the printed dimensions and the slicing results.

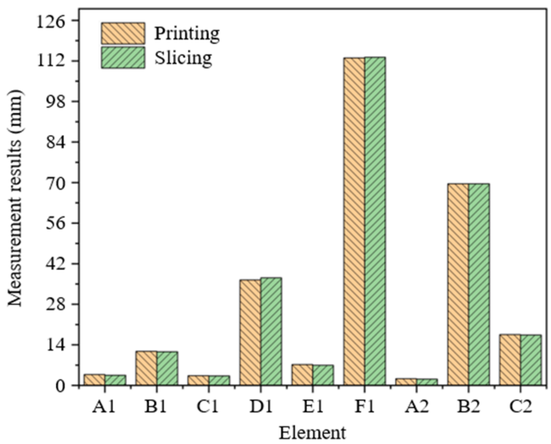

Fig. 12 Comparison of printed and slicing dimensions

From the graph above, the error value of the average measurements for the three printed specimens compared with slicing is below 2%. However, two elements have larger errors: 7.85% for element A1 and 6.89% for element A2. These elements are located in the height section of the printed specimen. This is caused by several factors, such as the layer-by-layer deposition process, which may result in gaps between layers. Therefore, it can be concluded that the printed results from the slicing and printing processes show significant errors in the height section. However, this is still considered acceptable, as the large deviations are likely due to the small comparison values, which cause the error to appear significantly larger when calculated. Next, in the sintering process, measurements were taken the same way as in the printing process. Fig. 13 compares the measurement results for each element in each specimen after sintering, using a vernier caliper.

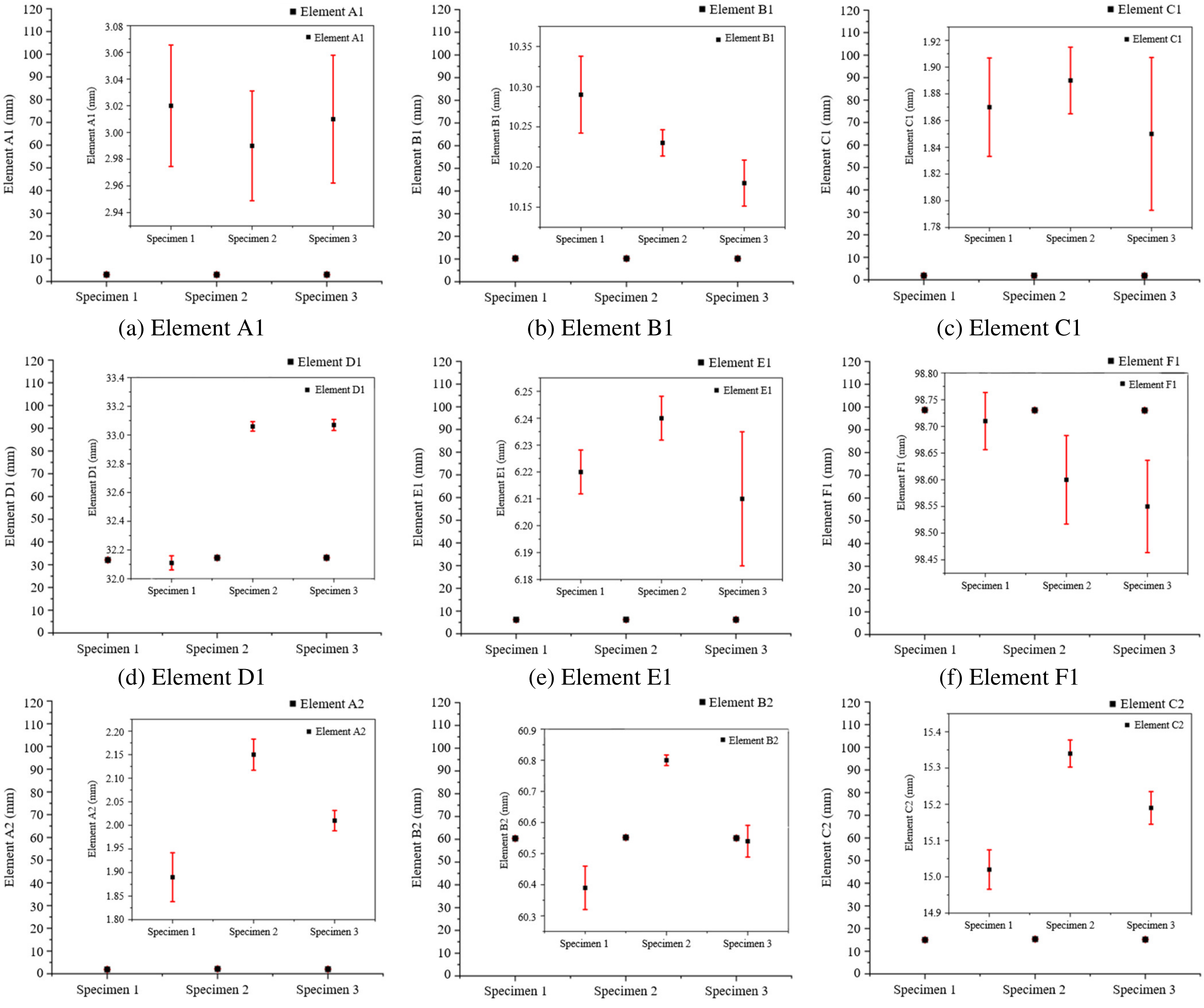

(a) Element A1 (b) Element B1 (c) Element C1

(d) Element D1 (e) Element E1 (f) Element F1

(g) Element A2 (h) Element B2 (i) Element C2

Fig. 13 Comparison of measured dimensions for three sintered specimens of each element

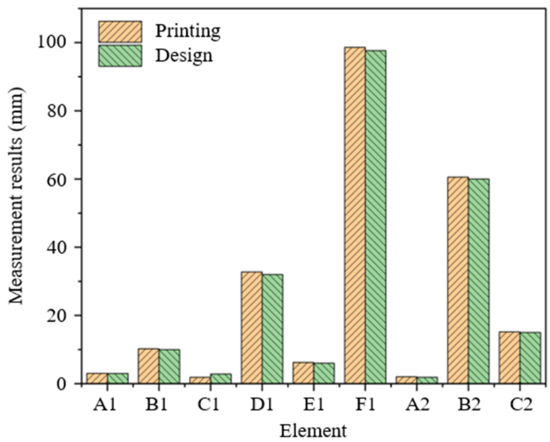

Fig. 14 Comparison of sintered dimensions and design

Based on the graph in Fig. 13, the deviation range shown is varied, similar to the measurement results in the printing process. This is due to factors in the sintering process that cannot be well-controlled, leading to uneven heat distribution during sintering, which makes it difficult to predict the outcome [19]. The limitations of this method should be revisited to achieve more accurate sintering results that meet the expected targets. However, looking at the measurement results of the sintered specimens using a vernier caliper, the pattern of values appears consistent, with no significant differences between the specimens post-sintering. This is a key advantage of the BMD method. It is important to note that the shapes used in this study are relatively simple and not complex, so there is a possibility that more complex designs could result in different outcomes. When compared with the design dimensions from the CAD software, as shown in Fig. 14, the comparison between the sintered dimensions and the design does not show significant differences.

As summarized in Table 7, both printed and sintered specimens exhibited low variability, with standard deviations generally <0.1 mm and a maximum of 0.43 mm. Percentage errors ranged from –1.94% to +7.76% for printed specimens (relative to slicing) and from –33.92% to +8.60% for sintered specimens (relative to CAD design). Notably, element C1 showed the largest relative error due to its small dimension, while absolute deviations remained within the sub-millimeter scale for most features.

Table 7 Printed and sintered specimen dimensions with standard deviation and % error

Element	Printed (mm)	Sintered (mm)	% Error of printed vs slicing	% Error of sintered vs CAD
A1	3.75 ± 0.04	3.01 ± 0.06	+7.76%	+0.33%
B1	11.78 ± 0.05	10.23 ± 0.05	+1.55%	+2.30%
C1	3.33 ± 0.16	1.87 ± 0.06	+1.44%	–33.92%
D1	36.40 ± 0.13	32.75 ± 0.43	–1.94%	+2.34%
E1	7.21 ± 0.06	6.22 ± 0.02	+3.59%	+3.67%
F1	113.05 ± 0.05	98.62 ± 0.10	–0.21%	+0.98%
A2	2.31 ± 0.08	2.02 ± 0.09	+7.06%	+8.60%
B2	69.58 ± 0.13	60.58 ± 0.21	–0.03%	+0.97%
C2	17.54 ± 0.02	15.18 ± 0.12	+0.81%	+1.20%

The error values vary from 0.03% to 33.9% when comparing the average sintered specimen with the design. The most significant error occurs in element C1, which can be attributed to the complexity of the measurement process and the challenges of sintering in curved areas, possibly causing slight size reductions compared to the design. However, this significant difference, similar to the printing process, may also be due to the small size of the element, which amplifies the error value when calculated. It should be noted that the absolute deviation for C1 was approximately 0.96 mm, and the low standard deviation across repeated measurements (±0.06 mm) indicates that this result is consistent and not a random measurement artifact. Beyond measurement complexity, the extreme shrinkage observed in element C1 can also be explained by geometry-dependent thermal gradients and binder-removal dynamics.

Thin and curved features such as C1 exhibit a higher surface-to-volume ratio, which leads to faster heat penetration and steeper local thermal gradients during sintering. These conditions accelerate binder removal in the early stages, leaving locally uneven porosity and enhancing densification once diffusion becomes dominant. As a result, C1 undergoes disproportionately large contraction compared to thicker or more uniform elements (e.g., D1 and F1), where thermal distribution is more homogeneous. The extreme shrinkage ratio of 1.78 thus reflects a systematic sensitivity of very small, curved features to anisotropic shrinkage during sintering, rather than a process anomaly. This suggests that special compensation strategies or design adjustments are necessary for features of this scale. The overall error pattern shows an average error of 6% from the original size. This is relatively large, suggesting that the design process and scale factor adjustments must be reconsidered to achieve better results during sintering.

To complement the percentage error analysis, absolute deviations in millimeters were also calculated to provide a more balanced assessment of dimensional accuracy. As summarized in Table 7, absolute deviations ranged from 0.01 mm (A1) to 0.96 mm (C1 and F1). This shows that although C1 exhibited a large percentage error of –33.92%, the actual deviation was less than 1 mm, which is clinically more meaningful. Conversely, larger features such as F1 exhibited nearly 1 mm deviation, yet this corresponded to only +0.98% relative error, demonstrating that percentage error can exaggerate dimensional differences in small features while underrepresenting them in larger ones.

To further quantify overall accuracy, a normalized root-mean-square error (NRMSE) was calculated as:

$$\text{NRMSE} = \frac{\sqrt{\frac{1}{n}\sum_{i=1}^{n}\left(x_i - y_i\right)^2}}{x_{\max} - x_{\min}} \tag{2}$$

where x_i and y_i represent the reference (CAD or slicing) and the measured values (printed or sintered), respectively. The NRMSE values were 0.0027 (0.27%) for the slicing-to-printing comparison and 0.0059 (0.59%) for the CAD-to-sintered comparison, confirming that global dimensional deviations remained below 1% of the overall size range. While maximum allowable dimensional errors are not universally defined, prior dental studies have reported acceptable deviations of 0.19 to 0.23 mm at the entry point and 0.32 to 0.36 mm at the apex of implants, as well as up to 0.26 mm for dental models [13, 20]. Thus, the observed deviations in this study fall within the same order of magnitude as established clinical tolerances, supporting the practical relevance of the refined 1.13 scale factor.

BMD has critical implications for the clinical fit of patient-specific implants. In orthopedic applications, unanticipated shape and size deviations can reduce mechanical stability and lead to complications such as wound dehiscence, infection, or implant dislocation [13]. In dental implants, even sub-millimeter deviations can disrupt placement accuracy, affect occlusion, and potentially decrease procedural success [14-15]. Maximum allowable dimensional errors for clinical use are not universally defined; however, dental research suggests entry point offsets of 0.19 to 0.23 mm and apex offsets of 0.32 to 0.36 mm are clinically acceptable [13]. For dental models, deviations up to 0.26 mm remain within tolerance [20]. Although precise fit is crucial in orthopedic applications, standardized regulatory limits are still lacking, highlighting the need for further evidence-based studies [16].

Furthermore, factors influencing dimensional deviations include printing technology, build orientation, and layer height, with digital light processing (DLP) printers showing superior accuracy in dental model fabrication compared to other techniques [14-15]. The accuracy of 3D printed surgical templates also depends on implant-analog positioning and printing parameters [18]. These results emphasize the need for process optimization and accurate scale factor application to minimize dimensional errors, ensuring implants meet medical applications' stringent safety and functional requirements.

Based on the comparison between the CAD design, printed results, and final sintered dimensions, it was found that the initially applied scale factor of 1.16 was insufficient to ensure that the final sintered dimensions matched the original design accurately. To assess the actual dimensional shrinkage during the transition from printing to sintering, a shrinkage ratio was calculated as follows.

$$\text{Shrinkage ratio} = \frac{\text{Printed results}}{\text{Sintered results}} \tag{3}$$

where printed result refers to the dimensions obtained from the printing process, and sintered specimen refers to the dimensions of each element after the sintering process. The shrinkage ratio data between the printed and sintered specimens are summarized in Table 8.

Table 8 Shrinkage ratio of the printed result relative to the sintered specimen

Element	Printed result	Sintered specimen	Shrinkage ratio
A1	3.75 mm	3.01 mm	1.25
B1	11.78 mm	10.23 mm	1.15
C1	3.33 mm	1.87 mm	1.78
D1	36.4 mm	32.75 mm	1.11
E1	7.21 mm	6.22 mm	1.16
F1	113.05 mm	98.62 mm	1.15
A2	2.31 mm	2.02 mm	1.14
B2	69.58 mm	60.58 mm	1.15
C2	17.54 mm	15.18 mm	1.15

The average shrinkage ratio across all elements is 1.22, which generally indicates that the specimen experienced greater shrinkage than what was compensated for by the design scale factor of 1.16. However, it is essential to note that this value is significantly influenced by element C1, which exhibits an extreme shrinkage ratio of 1.78. If element C1 is excluded from the calculation, the average shrinkage ratio drops to 1.16, matching the scale factor applied in the initial design. This suggests that the initial design approach is sufficiently accurate for most elements, but small and complex elements like C1 may require special treatment or specific adjustment [21]. To obtain final dimensions that more closely match the original design, a new scale factor was calculated based on the actual sintered dimensions relative to the design dimensions.

$$R_1 = R_0 \times \left(\frac{N_0}{N_1} \right) \tag{4}$$

where R_1 is the new scale factor, R_0 is the initial scale factor, N_0 is the dimension of each element in the design, and N_1 is the dimension of each component after sintering. The calculation results are presented in Table 9.

Table 9 New scale factor based on sintered specimen relative to the design

Element	Designed dimension	Sintered specimen	New scale factor
A1	3 mm	3.01 mm	1.15
B1	10 mm	10.23 mm	1.13
C1	2.83 mm	1.87 mm	1.75
D1	32 mm	32.75 mm	1.13
E1	6 mm	6.22 mm	1.12
F1	97.66 mm	98.62 mm	1.15
A2	1.86 mm	2.02 mm	1.07
B2	60 mm	60.58 mm	1.15
C2	15 mm	15.18 mm	1.15

The average newly obtained scale factor is 1.13, which is lower than the initial value of 1.16 when excluding element C1. This indicates that a reduction in the design scale factor is necessary to achieve more accurate design dimensions after sintering, particularly for elements that closely approach or exceed the target dimensions, such as A2 and B1. Elements with more significant deviations, such as C1, require special strategies regarding geometric design, printing orientation, or more controlled sintering processes.

To further illustrate the practical effect of this adjustment, a sensitivity analysis was performed by comparing deviations of representative elements with clinical tolerances. For instance, element B1 showed a deviation of +0.23 mm relative to the design, which remains within the clinically acceptable limit for dental entry points (0.19 to 0.23 mm). In contrast, element C1 exhibited a shrinkage of –0.96 mm, far exceeding tolerance thresholds, suggesting that extremely small and curved features are disproportionately sensitive to shrinkage. Meanwhile, larger elements such as F1 deviated only +0.96 mm over a 97.66 mm length (≈0.9%), indicating that bulk dimensions are less affected. These findings demonstrate that applying the refined scale factor of 1.13 improves dimensional fidelity for most features but that certain geometries still require additional design or process-specific compensation.

These findings are consistent with previous studies showing that the sintering process in BMD technology exhibits varying shrinkage behavior depending on geometry, thermal mass, and print orientation [19]. Compared to methods such as MIM or SLM, the variations in BMD are more complex due to thermally degraded binders rather than direct melting. Therefore, empirically based compensation approaches are crucial to ensure competitiveness in high-precision applications [22]. Unlike earlier studies that mainly addressed shrinkage at the sintering stage or proposed partial compensation models [9, 12, 18], the present study provides a full-chain dimensional assessment covering design, slicing, printing, and sintering, validated by both experimental and simulation results, and explicitly linked to clinical tolerances.

In comparison, SLM achieves high-dimensional fidelity due to precise control over process parameters such as laser energy, layer thickness, and build orientation [23]. BJ, on the other hand, typically shows greater dimensional deviations and inhomogeneous shrinkage up to 20% during the sintering stage, especially when binder saturation and thermal treatment are not well optimized [24]. The dimensional precision of BJ ranges from IT9 to IT15, which is lower than that achievable by SLM [24]. BMD sits between these techniques; while it currently presents larger deviations, the application of optimized scale factors, as demonstrated in this study, improves dimensional fidelity and makes BMD viable for cost-sensitive, complex part production in medical contexts [25].

Inaccuracies between the design and the final result due to improper scale factors can have significant consequences, especially in medical applications such as fabricating patient-specific anatomical implants. In this context, even minimal dimensional deviations can lead to geometric mismatch with the patient's biological structures, impair biomechanical function, or even result in clinical failure [13, 26]. Hence, the calibration and validation of scale factors during the design phase are critical to ensuring accuracy, safety, and success in medical applications.

4.2. Sintering simulation analysis

To verify the shrinkage ratio obtained through experimental methods, a sintering simulation was conducted to clarify the experimental calculations and improve data accuracy. This simulation was performed using ANSYS 2022 R2 software, utilizing Transient Thermal and Static Structural features to obtain the specimen's deformation. Based on the simulation results, the shrinkage values could be determined. The material specifications and simulation parameters were based on the datasheets provided by Desktop Metal and previous researchers [27], as presented in Table 10. In addition, the ANSYS simulation was conducted using a transient thermal–structural coupling approach. A tetrahedral mesh with an average element size of 0.5 mm was generated, refined locally at curved features such as C1. Boundary conditions included a fixed constraint at the specimen base and a heat flux applied to the external surfaces, following Eq. (4) and the formula described below. The time-step size was set to 1 s with automatic adjustment to ensure stability, and convergence was achieved when residuals for energy and displacement dropped below 1×10^{-3}.

Table 10 New scale factor based on sintered specimen relative to the design

Temperature (°C)	Specific heat (kJ/kg/°C)	Thermal conductivity (W/m/°C)	Thermal expansion ($\times 10^{-6}$ mm/mm/°C)
1380	0.659	33.78	20.21

Several input parameters must be defined in the simulation to obtain results that accurately reflect the conditions of the experimental process. One essential input is the heat flux value. This heat flux can be determined using Fourier's Law [28], as described by the following formulas. Fourier's Law was applied to compute the transient heat flux within the specimen during sintering. The resulting temperature gradients provided the thermal input that drives diffusion and sintering stress, which in turn cause densification and shrinkage. In this way, the following formulas directly feed into the shrinkage model by linking heat transfer to dimensional change.

$$q = -k \times \frac{dT}{dx} \tag{5}$$

$$q = -k \times \frac{\Delta T}{L} \tag{6}$$

where q is the heat flux (W/mm^2), k is the thermal conductivity (W/m/°C), ΔT is the temperature difference (°C), and L is the effective thickness of the specimen in the direction of heat transfer (mm). To ensure continuity between the experimental and numerical analyses, the experimentally obtained shrinkage ratios and the refined scale factor of 1.13 were used as validation benchmarks for the ANSYS simulation. The simulation boundary conditions were defined to replicate the furnace environment: the specimen base was constrained to represent its contact with the platform, and all exposed surfaces were subjected to a uniform heat flux.

The applied heat flux magnitude was 30.52 W/mm^2 for the tensile specimen and 49.22 W/mm^2 for the bending specimen, calculated using Fourier's Law with the furnace temperature (1380 °C), the measured specimen thicknesses of 1.5 mm and 0.93 mm. Material properties, including thermal conductivity, specific heat capacity, and thermal expansion coefficient (Table 10), were taken directly from the Desktop Metal datasheet and literature, ensuring realistic thermal–structural coupling. The sintering was carried out in an H_2+Ar inert atmosphere, minimizing external convection, which justifies the assumption of uniform thermal loading. These combined inputs ensured that the simulation setup closely corresponded to the actual sintering process.

Furthermore, to determine the relationship between the scale factor and the heat flux value, it is linked with the linear thermal expansion formula [29]. The direct link between Fourier's Law and shrinkage lies in the fact that heat flux determines the transient thermal gradients within the specimen. These gradients drive diffusion and porosity elimination during sintering, leading to densification and dimensional contraction. By combining the Fourier-derived heat flux with the thermal expansion–contraction relations, the simulation establishes a mechanistic pathway from heat transfer to shrinkage prediction.

$$\Delta T = \alpha \times L_0 \times \Delta T \tag{7}$$

$$L_{final} = L_0 + \Delta L = L_0 \times (1 + \alpha \times \Delta T) \tag{8}$$

$$\text{Ratio} = \frac{L_{final}}{L_0} = 1 + \alpha \times \Delta T \tag{9}$$

$$\text{Ratio} = 1 + \alpha \times \left(\frac{q \times L}{k} \right) \tag{10}$$

where Ratio is the comparison between the initial scale factor and the shrinkage result, and α is the coefficient of thermal expansion (C^{-1}). The relationship between the scale factor input and the heat flux input in the ANSYS 2022 R2 software is established using these formulas. Based on the calculated scale factor of 1.16, the simulation results are presented in Fig. 15.

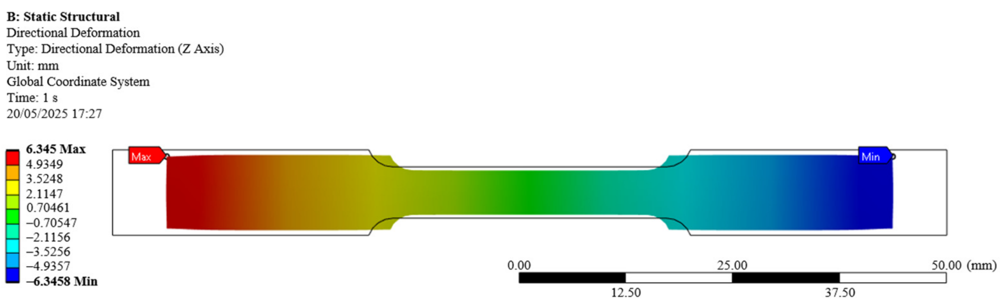

(a) Tensile test specimen

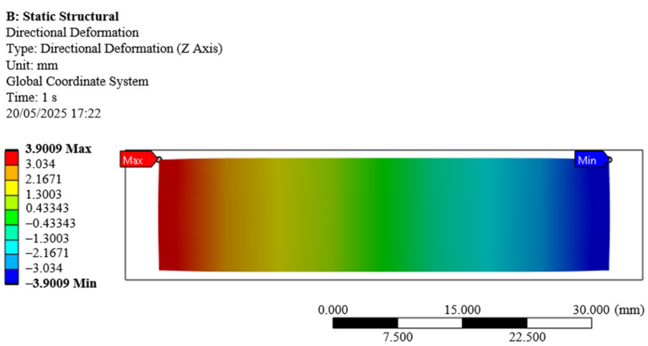

(b) Bending test specimen

Fig. 15 Simulation results

The specimen shrinkage was obtained from the simulation results by reducing the scaled design size of 1.16 back to its original size. The observed shrinkage behavior corresponds closely with experimental findings, confirming the validity of the applied thermal and structural parameters. These results provide a quantitative reference for correlating the heat flux distribution with dimensional contraction, ensuring that the simulated outcomes accurately represent the real sintering conditions. The detailed results for each element are shown in Table 11.

Table 11 Simulated shrinkage results and scale factors for each element

Element	Design scale factor	Simulated shrinkage result	Shrinkage scale factor
A1	3.48 mm	3.09 mm	1.13
B1	11.6 mm	10.3 mm	1.13
C1	3.28 mm	2.92 mm	1.13
D1	37.12 mm	32.96 mm	1.13
E1	6.96 mm	6.18 mm	1.13
F1	113.29 mm	100.6 mm	1.13
A2	2.16 mm	1.92 mm	1.13
B2	69.6 mm	61.8 mm	1.13
C2	17.4 mm	15.45 mm	1.13

Upon analysis, the simulation results indicate a shrinkage corresponding to a scale factor of 1.13. Therefore, a follow-up simulation is necessary to verify whether a scale factor of 1.13 will produce shrinkage that matches the original design dimensions. Table 12 provides detailed simulation results using a scale factor of 1.13.

Table 12 Simulation results using a scale factor of 1.13

Element	Scaled design dimension	Simulated shrinkage result	Shrinkage scale factor
A1	3.39 mm	3 mm	1.13
B1	11.3 mm	10 mm	1.13
C1	3.19 mm	2.83 mm	1.13
D1	36.16 mm	32 mm	1.13
E1	6.78 mm	6 mm	1.13
F1	110.35 mm	97.66 mm	1.13
A2	2.10 mm	1.86 mm	1.13
B2	67.8 mm	60 mm	1.13
C2	16.95 mm	15 mm	1.13

The table shows that a scale factor of 1.13 results in shrinkage that aligns with the original design dimensions. Therefore, to achieve optimal printing accuracy, a scale factor of 1.13 should be applied in the experimental process. Despite these promising findings, several limitations of the present study must be acknowledged. The number of tested specimens was relatively small, restricting the statistical generalization of dimensional deviations. Only simple geometries (tensile and bending specimens) were investigated, so the applicability of the refined scale factor to complex implant geometries remains untested. The simulation also employed simplified assumptions, such as uniform heat flux and an idealized furnace atmosphere, whereas actual sintering may involve more complex thermal interactions. Furthermore, the refined scale factor of 1.13 was derived under specific material (SS316L) and equipment (Desktop Metal BMD) conditions, and its transferability to other alloys or BMD systems remains to be validated. Finally, the clinical relevance was inferred indirectly from published dimensional tolerances rather than confirmed through direct in vitro or in vivo validation.

5. Conclusions

This study successfully conducted a comprehensive dimensional evaluation of 316L stainless steel specimens produced using the BMD method. The key findings are:

(1) Dimensional deviation of up to 6% was observed from CAD design to the final sintered product, with the most significant errors occurring in height-related features due to anisotropic shrinkage and irregular layer deposition.

(2) The commonly used scale factor of 1.16 was found to be suboptimal, resulting in inconsistent dimensional fidelity, particularly in smaller or curved features.

(3) Based on experimental and simulation results, a new refined scale factor of 1.13 was proposed. This factor demonstrated better alignment with the original design dimensions and was confirmed through ANSYS-based simulation.

(4) The proposed 1.13 scale factor achieved dimensional accuracy within the clinically acceptable tolerance for dental implants (0.19-0.36 mm), indicating its applicability in biomedical implant manufacturing.

(5) Simulation results further confirmed the superiority of scale factor 1.13, ensuring improved predictability of shrinkage and better control over the final output geometry.

(6) Comparison with other AM technologies showed that BMD has moderate dimensional accuracy, which can be enhanced through empirical compensation strategies, especially for cost-sensitive medical applications.

(7) The study emphasizes the importance of scale factor calibration in improving accuracy, safety, and performance in medical 3D-printed implants.

Overall, this study highlights a proof-of-concept that the refined scale factor can ensure clinically reliable dimensional accuracy for implant applications. Future studies should further validate and extend the applicability of the proposed scale factor and dimensional control methods in BMD. Future work should aim to:

(1) Experimental validation of the 1.13 scale factor under real clinical manufacturing conditions, with a larger sample size to improve statistical confidence and capture process variability.

(2) Investigation of more complex geometries and loading scenarios to improve the general applicability of the proposed calibration method.

Conflicts of Interest

The authors declare no conflict of interest.

References

[1] "BRIN Kembangkan Riset Material untuk Implan Tulang," https://www.brin.go.id/news/110583/brin-kembangkan-riset-material-untuk-implan-tulang, 2022.
[2] C. Morsiya, "A Review on Parameters Affecting Properties of Biomaterial SS 316L," Australian Journal of Mechanical Engineering, vol. 20, no. 3, pp. 803-813, 2022.
[3] J. Petrusa, B. Meier, G. Grünbacher, W. Waldhauser, and J. Eckert, "Surface Topography and Biocompatibility of CP–Ti Grade2 Fabricated by Laser-Based Powder Bed Fusion: Influence of Printing Orientation and Surface Treatments," Advanced Engineering Materials, vol. 25, no. 7, article no. 2201073, 2023.
[4] Y. K. P. Saleh, R. Ismail, J. Jamari, I. N. Jujur, S. Suryadi, R. Winarso, et al., "Finite Element Analysis of Ti-6Al-4V Lattice Cubic Scaffolds for Mandibular Bone Implant Applications," Advances in Technology Innovation, vol. 10, no. 3, pp. 283-295, 2025.
[5] B. Iacopo, D. P. Valerio, M. Tommaso, P. Massimiliano, and V. Alessio, "Environmental Impacts Assessment of Bound Metal Deposition 3D Printing Process for Stainless Steel," Procedia CIRP, vol. 105, pp. 386-391, 2022.
[6] A. Watson, J. Belding, and B. D. Ellis, "Characterization of 17-4 PH Processed via Bound Metal Deposition (BMD)," TMS 2020 149th Annual Meeting & Exhibition Supplemental Proceedings, pp. 205-216, 2020.
[7] F. Bjørheim and I. M. L. T. Lopez, "Tension Testing of Additively Manufactured Specimens of 17-4 PH Processed by Bound Metal Deposition," IOP Conference Series: Materials Science and Engineering, vol. 1201, article no. 012037, 2021.
[8] Q. Campbell, M. Filiault, K. Rooney, J. Belding, and B. D. Ellis, "Design and Manufacture of a Functional 3D-Printed Stirling Engine: A Case Study Involving Bound Metal Deposition of 17-4 PH," TechConnect Briefs, vol. 2019, pp. 139-142, 2019.
[9] D. G. Luchinsky, V. Hafiychuk, K. R. Wheeler, and T. J. Prater, "Analysis of Nonlinear Shrinkage for the Bound Metal Deposition Manufacturing Using Multi-Scale Approach," NASA, Technical Report TM-20210010310, 2021.

[10] V. V. P. Babu, G. B. V. Kumar, and P. Barmavatu, "Dimensional Accuracy Testing and Analysis of 3D Metal Printed SS316L Using DMLS Technique," International Journal on Interactive Design and Manufacturing, vol. 19, no. 1, pp. 375-392, 2025.

[11] W. Chen, Z. Chen, L. Chen, D. Zhu, and Z. Fu, "Optimization of Printing Parameters to Achieve High-Density 316L Stainless Steel Manufactured by Binder Jet 3D Printing," Journal of Materials Engineering and Performance, vol. 32, no. 8, pp. 3602-3616, 2023.

[12] Z. Chen, B. Wan, J. Liu, D. Zhu, H. Wang, W. Chen, et al., "Sintering Densification Mechanism of Binder Jet 3D Printing 316L Stainless Steel Parts via Dimensional Compensation Technology," Journal of Materials Research and Technology, vol. 33, pp. 3296-3307, 2024.

[13] A. P. McAnena, T. McClennen, and H. Zheng, "Patient-Specific 3-Dimensional-Printed Orthopedic Implants and Surgical Devices Are Potential Alternatives to Conventional Technology but Require Additional Characterization," Clinics in Orthopedic Surgery, vol. 17, no. 1, pp. 1-15, 2024.

[14] L. Herschdorfer, W. M. Negreiros, G. O. Gallucci, and A. Hamilton, "Comparison of the Accuracy of Implants Placed with CAD-CAM Surgical Templates Manufactured with Various 3D Printers: An In Vitro Study," The Journal of Prosthetic Dentistry, vol. 125, no. 6, pp. 905-910, 2021.

[15] F. Husain, V. Grover, N. Bhaskar, and A. Jain, "Comparative Evaluation of Accuracy of Implants Placed with Thermoplastic and Three-Dimensional-Printed Surgical Guides: A Randomized Controlled Trial," Journal of Indian Society of Periodontology, vol. 28, no. 2, pp. 244-251, 2024.

[16] A. Strunz, L. Berger, A. Seidel, J. Ries, W. Adler, M. Wichmann, et al., "The Impact of Three-Dimensional Printer Technology on the Accuracy of Dental Implant Models," Materials, vol. 18, no. 9, article no. 1902, 2025.

[17] U. Aziz, M. McAfee, I. Manolakis, N. Timmons, and D. Tormey, "A Review of Optimization of Additively Manufactured 316/316L Stainless Steel Process Parameters, Post-Processing Strategies, and Defect Mitigation," Materials (Basel), vol. 18, no. 12, article no. 2870, 2025.

[18] T. ElShebiny, S. Matthaios, L. M. Menezes, I. A. Tsolakis, and J. M. Palomo, "Effect of Printing Technology, Layer Height, and Orientation on Assessment of 3D-Printed Models," Journal of the World Federation of Orthodontists, vol. 13, no. 4, pp. 169-174, 2024.

[19] A. K. Basak, A. Pramanik, Y. X. Chen, C. Prakash, N. Radhika, and S. Shankar, "Bound Metal Deposition of Stainless Steel 316L: Effect of Process Variables on Microstructural and Mechanical Behaviors," Materialia, vol. 36, article no. 102196, 2024.

[20] L. E. Ritacco, F. E. Milano, and E. Chao, Computer-Assisted Musculoskeletal Surgery: Thinking and Executing in 3D, Cham: Springer, pp. 181-198, 2016.

[21] A. Pellegrini, M. G. Guerra, and F. Lavecchia, "Shrinkage Evaluation and Geometric Accuracy Assessment on 17–4 PH Samples Made by Material Extrusion Additive Manufacturing," Journal of Manufacturing Processes, vol. 109, pp. 394-406, 2024.

[22] N. Decker and Q. Huang, "Optimizing the Expected Utility of Shape Distortion Compensation Strategies for Additive Manufacturing," Procedia Manufacturing, vol. 53, pp. 348-358, 2021.

[23] X. Yang, Y. Yang, Y. Liu, and D. Wang, "Study on Dimensional Accuracy of Typical Geometric Features Manufactured by Selective Laser Melting," Chinese Journal of Lasers, vol. 42, no. 3, article no. 303004, 2015.

[24] M. Zago and I. Cristofolini, "Assessment of the Achievable Dimensional Tolerances in 17-4PH Stainless Steel Parts Fabricated by Metal Binder Jetting," Design Tools and Methods in Industrial Engineering III, pp. 31-40, 2023.

[25] K. Zhang, W. Zhang, R. Brune, E. Herderick, X. Zhang, J. Cornell, et al., "Numerical Simulation and Experimental Measurement of Pressureless Sintering of Stainless Steel Part Printed by Binder Jetting Additive Manufacturing," Additive Manufacturing, vol. 47, article no. 102330, 2021.

[26] R. A. Laynes and C. J. Kleck, "Patient-Specific Implants and Spinal Alignment Outcomes," North American Spine Society Journal, vol. 20, article no. 100559, 2024.

[27] A. Özcan, S. Kollmannsberger, J. Jomo, and E. Rank, "Residual Stresses in Metal Deposition Modeling: Discretizations of Higher Order," Computers & Mathematics with Applications, vol. 78, no. 7, pp. 2247-2266, 2019.

[28] Y. Wang and P. Wang, "Application of Fourier's Law in One-Dimensional Steady Heat Conduction Calculation of Cylinder Wall," Journal of Physics: Conference Series, vol. 2381, article no. 012002, 2022.

[29] N. A. Palii and O. K. Belousov, "Semi-Empirical Evaluation of Linear Coefficient of Thermal Expansion of Metals," Journal of Physics: Conference Series, vol. 1942, article no. 012022, 2021.